Article

Carbon Nitride Quantum Dots Modified TiO₂ Inverse Opal Photonic Crystal for Solving Indoor VOCs Pollution

Jie Yu [1,2], Angel Caravaca [2], Chantal Guillard [2], Philippe Vernoux [2], Liang Zhou [1,3], Lingzhi Wang [4], Juying Lei [1,3,5,*], Jinlong Zhang [4] and Yongdi Liu [1,3,5,*]

[1] National Engineering Laboratory for Industrial Wastewater Treatment, School of Resources and Environmental Engineering, East China University of Science and Technology, Shanghai 200237, China; jie.yu@ircelyon.univ-lyon1.fr (J.Y.); zhouliang@ecust.edu.cn (L.Z.)

[2] Institut de Recherches sur la Catalyse et l'Environnement de Lyon, UMR 5256, CNRS, Université Claude Bernard Lyon 1, CNRS, IRCELYON, F-69626 Villeurbanne, France; angel.caravaca@ircelyon.univ-lyon1.fr (A.C.); chantal.guillard@ircelyon.univ-lyon1.fr (C.G.); philippe.vernoux@ircelyon.univ-lyon1.fr (P.V.)

[3] State Environmental Protection Key Laboratory of Environmental Risk Assessment and Control on Chemical Process, School of Resources and Environmental Engineering, East China University of Science and Technology, Shanghai 200237, China

[4] Key Lab for Advanced Materials and Institute of Fine Chemicals, East China University of Science and Technology, Shanghai 200237, China; wlz@ecust.edu.cn (L.W.); jlzhang@ecust.edu.cn (J.Z.)

[5] Shanghai Institute of Pollution Control and Ecological Security, Shanghai 200237, China

[*] Correspondence: leijuying@ecust.edu.cn (J.L.); ydliu@ecust.edu.cn (Y.L.)

Abstract: Indoor toxic volatile organic compounds (VOCs) pollution is a serious threat to people's health and toluene is a typical representative. In this study, we developed a composite photocatalyst of carbon nitride quantum dots (CNQDs) in situ-doped TiO₂ inverse opal TiO₂ IO for efficient degradation of toluene. The catalyst was fabricated using a sol-gel method with colloidal photonic crystals as the template. The as-prepared catalyst exhibited excellent photocatalytic performance for degradation of toluene. After 6 h of simulated sunlight irradiation, 93% of toluene can be converted into non-toxic products CO_2 and H_2O, while only 37% of toluene is degraded over commercial P25 in the same condition. This greatly enhanced photocatalytic activity results from two aspects: (i) the inverse opal structure enhances the light harvesting while providing adequate surface area for effective oxidation reactions; (ii) the incorporation of CNQDs in the framework of TiO₂ increases visible light absorption and promotes the separation of photo-generated charges. Collectively, highly efficient photocatalytic degradation of toluene has been achieved. In addition, it can be expanded to efficient degradation of organic pollutants in liquid phase such as phenol and Rhodamine B. This study provides a green, energy saving solution for indoor toxic VOCs removal as well as for the treatment of organic wastewater.

Keywords: carbon nitride; quantum dots; inverse opal; photocatalysis

1. Introduction

Nowadays, people spend most of their time (up to 90%) in an indoor environment. Thus, indoor air quality (IAQ) has a significant influence on human health, comfort and productivity [1,2]. Indoor air pollution is now considered among the top five environmental risks to public health according to the Environmental Protection Agency (EPA), which declared the air to be two to five times more polluted indoors than outdoors [3]. Interior flooring, adhesives, etc., used in interior decoration are sources of volatile organic compounds (VOCs) [4,5]. Exposure to toxic VOCs is seriously harmful to human health. In the past, benzene was widely used as an organic solvent for adhesives and paints. Nowadays, benzene has been replaced by relatively less toxic solvents, such as toluene, owing to its carcinogenic property [6]. However, toluene emitted from building materials

to indoor environments is known to cause several sick house syndromes, including vertigo, headache, nausea and allergies. Due to the gravity of the situation, people's requirements for clean and safe indoor circumstances have rapidly increased. Many technologies have been developed for removing VOCs from indoor air, such as adsorption [7], ozonation [8] and non-thermal plasma [9]. However, these treatment methods are highly expensive and can cause the production of a secondary pollution of hazardous compounds. Photocatalytic oxidation using light irradiation [10] allows us to completely degrade organic pollutants to small and non-hazardous molecules (CO_2 and H_2O) and has, therefore, been suggested as an attractive alternative to solve the indoor pollution issue [11].

In this sense, for the past decade, photonic crystals (PCs) have received a great deal of attention to improve the conversion of photochemical energy by enhancing the interaction of light and matter without chemical modification [12]. Most TiO_2 PCs are also called inverse opals (IOs) because they are made by colloidal self-assembly followed by structural inversion [13]. IO structures can improve light collection efficiency through multiple scattering [14–17], slow light effect [18,19] and other mechanisms. PC structures are widely used in many fields, such as surface enhanced Raman (SERS) detection [20], battery electrodes [21], solar cell [22], photocatalysis [23–25], etc. However, to the best of our knowledge there are few reports about applying photocatalysts with photonic crystal structures for the degradation of VOCs.

Due to its strong oxidation capacity, TiO_2 is widely used in the photocatalytic degradation of VOCs [26–28]. However, the band gap of TiO_2 is 3.2 eV, which limits the utilization efficiency of sunlight [29–31]. Graphitic carbon nitride (g-C_3N_4), as a metal-free semiconductor with band gap of 2.7 eV and excellent chemical stability [32], has been widely investigated in photocatalytic hydrogen production with water [33], degradation of organic pollutants [34–38], oxidation of alcohols [39], reduction of oxygen [40], etc. Recently, graphitic carbon nitride quantum dots (CNQDs) with excellent biocompatibility and optical properties [41] which can improve solar energy harvesting, were synthesized by a low-temperature solid-phase method [42]. It is promising to combine CNQDs with TiO_2 inverse opal photonic crystals to form a composite photocatalyst for improving the utilization of visible light as well as the surface interface charge transfer efficiency of photo-generated charge carriers.

Hence, we developed a novel photocatalyst of CNQDs in situ-modified TiO_2 inverse opal (TCN IO) by a simple sol-gel method. In this architecture, inverse opal structure can increase the specific surface area and the utilization rate of visible light. Furthermore, the modification of CNQDs helps to decrease the recombination rate of light-induced excitons. The photocatalytic activities of the samples were evaluated by the photocatalytic oxidation of toluene, a gas phase VOC, and phenol, a liquid phase pollutant, under simulated sunlight irradiation, and it was extended to the degradation of other organic pollutants in aqueous solution such as a typical dye pollutant Rhodamine B (RhB). It was found that the TCN IO exhibited significantly higher photocatalytic activity than TiO_2 IO, P25 and bulk-TiO_2 for VOCs removal. A highly efficient system for the degradation of VOCs by solar light was constructed, which provides an environmentally friendly solution for indoor toxic VOCs removal. In addition, TCN IO was also demonstrated to be efficient for the degradation of other organic pollutants in aqueous solution, such as the liquid phase VOCs pollutant phenol and the typical dye pollutant RhB; this suggests good prospective applications for the treatment of organic wastewater.

2. Results and Discussion

CNQDs with uniform small size were successfully prepared via a simple low-temperature solid-phase and dialysis method [42]. From Figure 1a,b, we can see that the sizes of as-synthesized CNQDs are in the range from 2 to 8 nm. Nano-sized CNQDs mixed with the Ti precursor solution can easily infuse into the porosity of PS spheres (Figure S1a). After calcination at 500 °C for 2 h to remove the template, TCN IO with the regular and ordered nanostructure was obtained as presented in Figure 1c. Similar structures were obtained

for TiO_2 IO (Figure S1b). It can be observed from the high-resolution transmission electron microscopy (HRTEM) image in Figure 1d that TCN IO depicted two different lattices. One lattice spacing is 0.361 nm, which corresponds to the (101) planes of TiO_2; the other is 0.346 nm, corresponding to the (002) planes of CNQDs, proving that CNQDs were successfully loaded into the skeleton of TiO_2 IO.
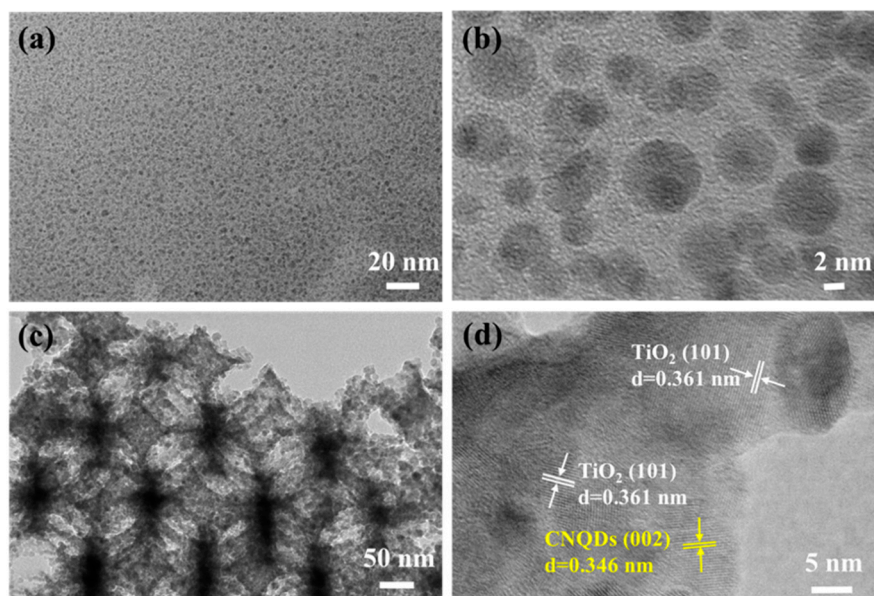

Figure 1. HRTEM images of (**a**,**b**) carbon nitride quantum dots (CNQDs) and (**c**,**d**) in situ-modified TiO_2 inverse opal (TCN IO).

The specific surface area is one of the vital factors that affects the photocatalytic performance of materials. Generally, the photocatalysts with larger surface areas possess more adsorption and active sites for photocatalytic process, which enhances the photocatalytic activity. N_2 sorption was carried out to determine the specific surface area as well as corresponding pore structure and to calculate the corresponding pore size distributions. As shown in Figure 2a, all samples exhibit type IV isotherms. TCN IO and TiO_2 IO display higher adsorption capacities at high relative pressures ($P/P_0 > 0.8$) than bulk-TiO_2, which provides evidence for the existence of macropores. The BJH pore size distribution (Figure 2b) reveals that the majority of the macropores have an average pore size of around 60 nm which provides larger surface areas and pore volumes than those of common bulk-TiO_2. The corresponding structural parameters of the as-synthesized samples obtained from the adsorption isotherms are summarized in Table 1.
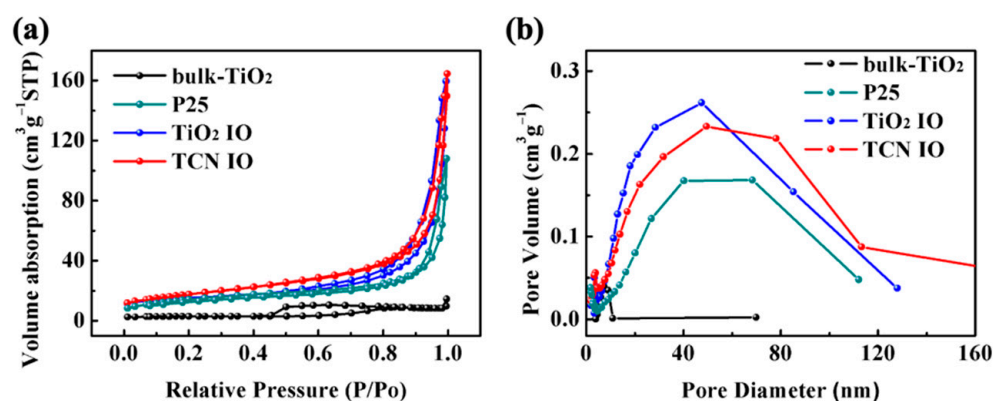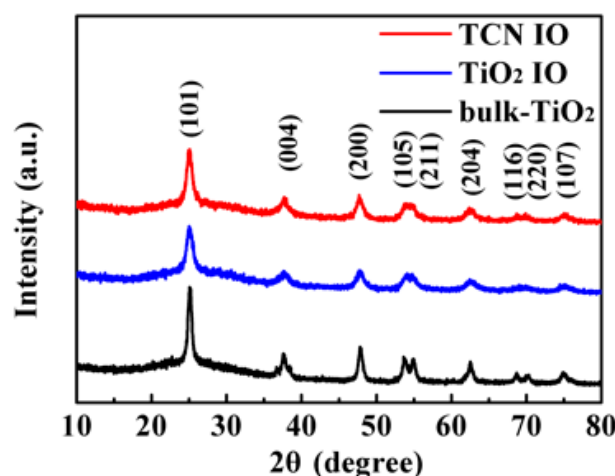

Figure 2. Nitrogen adsorption-desorption isotherms (**a**) and the corresponding pore size distribution curves (**b**) of bulk-TiO_2, TiO_2 IO, TCN IO, P25 sample, respectively.

Table 1. Brunauer−Emmett−Teller surface area (SBET) and pore volume of the photocatalysts.

Sample	SBET (m^2 g^{-1})	V Pore (cm^3 g^{-1})
bulk-TiO$_2$	9.0	0.022
P25	50.8	0.167
TiO2 IO	47.7	0.246
TCN IO	62.6	0.254

As shown in Table 1, the BET surface areas are approximately 9.0, 50.8, 47.7 and 62.6 m^2 g^{-1} for bulk-TiO$_2$, P25, TiO$_2$ IO and TCN IO, respectively. These results show that the inverse opal structure can increase the specific surface area of the material, while the introduction of CNQDs can further increase it. This could be attributed to the fact that nanosized CNQDs exhibit relatively high specific surface area. Additionally, the corresponding pore volume increases from 0.022 cm^3 g^{-1} for bulk-TiO$_2$ to 0.245 cm^3 g^{-1} for TiO$_2$ IO and to 0.254 cm^3 g^{-1} for TCN IO while the pore volume of P25 is 0.167 cm^3 g^{-1}. This can be attributed to the introduction of inverse opal structure, whose three-dimension-ordered pore structure benefits the enlargement of pore volume [43].

Figure 3 shows the X-ray diffraction (XRD) patterns of bulk-TiO$_2$, TiO$_2$ IO and TCN IO porous composites. For all samples, the XRD patterns exhibited strong diffraction peaks at 25.3° and 48°, indicating TiO$_2$ in the samples are all in anatase phase [25,29,44]. For CNQDs loaded TiO$_2$ IO composites (TCN IO), no diffraction peaks were observed for g-C$_3$N$_4$, most probably due to low weight loading and high dispersion of CNQDs in the catalyst.

Figure 3. X-ray diffraction (XRD) of samples.

X-ray photoelectron spectroscopy (XPS) spectra were used to analyze the elemental composition and the chemical state of elements in TCN IO. As Figure 4a shows, the XPS survey spectrum of TCN IO confirmed the existence of Ti, O, C and N elements. C 1s (Figure 4b) peak at 284.5 eV is assigned to the C-C bond in the turbostratic CN structure [36]. The C 1s peak at 285.8 eV is attributed to the sp2 C atoms bonded to N inside the aromatic structure. The peak at 288.5 eV is linked to the sp3 C-N bond of the sp3 bonded composition [45]. The N 1s peaks (Figure 4c) contain three components concentrated at 399.1 eV, 400.0 eV and 401.3 eV, which are identified as the C-N-C, (N (C)$_3$) and C-N-H groups, respectively [46]. The O 1s core level peak at 529.7 eV belongs to Ti-O-Ti linkages in TiO$_2$ (Figure 4d) [47]. After the modification of CNQDs, the peak at 531.4 eV, coming from OH functional groups on the surface of CNQDs, can be clearly identified. This latter peak is much higher than that of TiO$_2$ IO, revealing the successful loading of CNQDs to TiO$_2$ IO [48]. The XPS results of C 1s and N 1s further indicate the successful combination of CNQDs and TiO$_2$ IO.
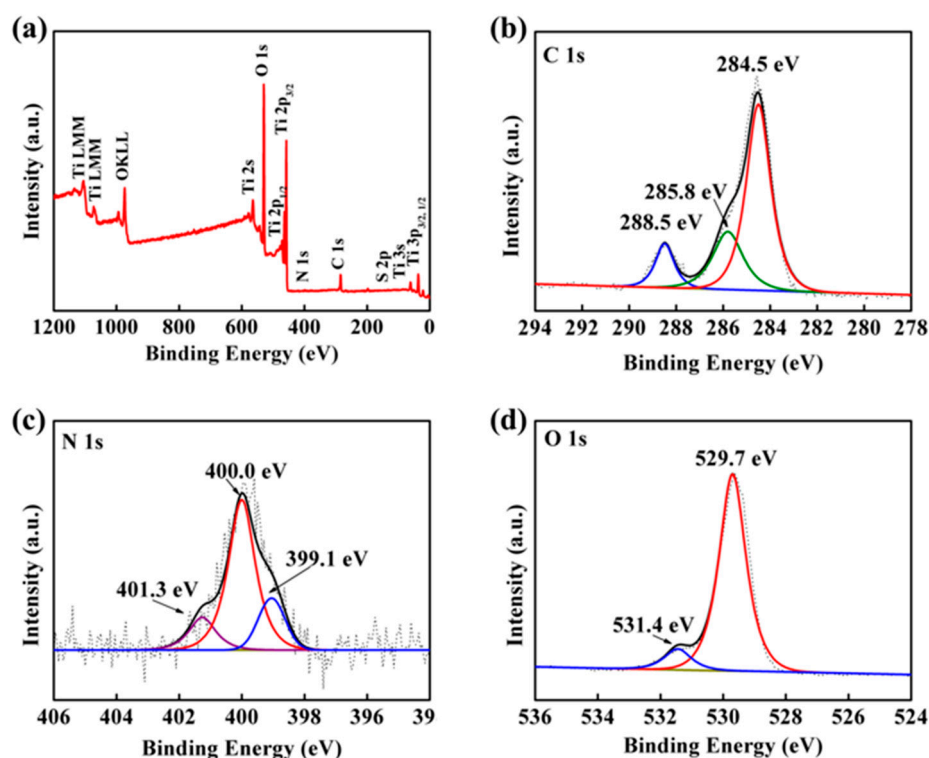
Figure 4. XPS survey spectrum (**a**) and corresponding core level spectra (**b**) C 1s, (**c**) N 1s and (**d**) O 1s of TCN IO.

The separation and transfer of electron-hole pairs of the samples can be analyzed via Electrochemical Impedance Spectroscopy (EIS) [49]. The intersection of the main high-frequency semicircle contribution with the x-axis in the Nyquist plots in EIS tests, corresponds to the charge transfer resistance of the catalysts. Figure 5a shows the Nyquist plots of TiO_2 IO and TCN IO electrodes, respectively. The EIS plot of TCN IO under simulated solar light illumination shows a smaller semicircular diameter compared with TiO_2 IO. This result indicates that TCN IO possess a smaller charge transfer resistance than that of TiO_2 IO without CNQDs modification. This suggests that the modification of CNQDs facilitates the charge separation efficiency of the catalyst. Photoluminescence (PL) spectra were analyzed (Figure 5b) to investigate the migration, transfer and recombination processes of the photo-generated electron-hole pairs in photocatalysts. Notably, the PL spectrum characteristics of the TiO_2 IO was markedly weaker than bulk-TiO_2. After the modification of CNQDs, PL intensity of TCN IO sample further weakens, which indicates a low recombination rate of photo-generated electrons and holes, and a favorable contact between CNQDs and TiO_2 IO. The construct of inverse opal structure and the introduction of CNQDs facilitate the faster separation of photo-generated charges, contributing to enhanced photocatalytic activity.

Samples were used for toluene degradation under AM1.5 simulated solar light irradiation (Figure 6). After 1 h dark adsorption, we assumed that the gas–solid adsorption equilibrium was reached, and the simulated sunlight irradiation began. The result of blank experiment (without any catalysts) confirms that the concentrations of CO_2 and toluene are stable (Figure 6a). In the dark, without the irradiation of simulated sunlight, the concentration of CO_2 did not increase, while that of toluene decreased. This is most probably due to the adsorption of the porous structure of TCN IO and the adsorption efficiency of TCN IO is 17% (Figure 6b). As shown in Figure 6c,d, the toluene concentration decreased as the illumination continued, and the concentration of CO_2 increased gradually, indicating that toluene was oxidized into CO_2. After 5h irradiation, 95% of toluene had been removed over TCN IO (Figure 6e), whereas the toluene removal rates of TiO_2 IO, bulk-TiO_2 and P25 were 88%, 77% and 60%, respectively. After 6 h irradiation, the concen-

tration of toluene is below the detection limit over TCN IO, whereas $C_{t, C7H8}$ drops to 17%, 2% and 37% of original concentration over bulk-TiO$_2$, TiO$_2$ IO and P25, respectively. Since the adsorption efficiency of TCN IO in the dark system is just 17%, the high removal rate of toluene obtained in the light irradiant system (100%) is mainly due to the photocatalytic degradation. Additionally, the calculated photocatalytic degradation efficiency of toluene into CO$_2$ (■$_{t, toluene}$) over bulk-TiO$_2$ is 60%, ■$_{t, toluene}$ is greatly improved to 82% after the introduction of inverse opal structure (Table S1). These results demonstrate that TiO$_2$ with inverse opal structure exhibits a significantly enhanced photocatalytic activity for the degradation of toluene under simulated sunlight compared to bulk-TiO$_2$. TCN IO shows the highest value of ■$_{t, toluene}$, up to 93%, while that of P25 is only 37%, revealing that the incorporation of inverse opal structure and CNQDs promotes the photocatalytic performance of the catalyst. The highly efficient activity of TCN IO can be explained by (i) the inverse opal structure which provides an adequate surface area for the adsorption and the oxidation of toluene; (ii) and the incorporation of CNQDs in the framework of TiO$_2$ which promotes the separation of photo-generated charges.
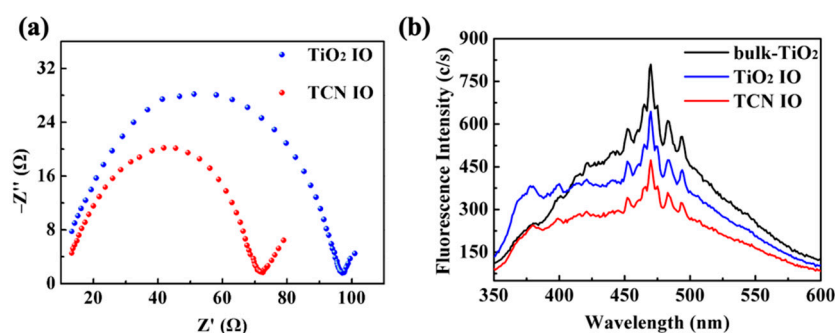

Figure 5. (**a**) Comparison of the electrochemical impedance spectroscopy (EIS) Nyquist plots for TiO$_2$ IO and TCN IO, (**b**) PL spectra of the photocatalysts (λ_{ex} = 360 nm).
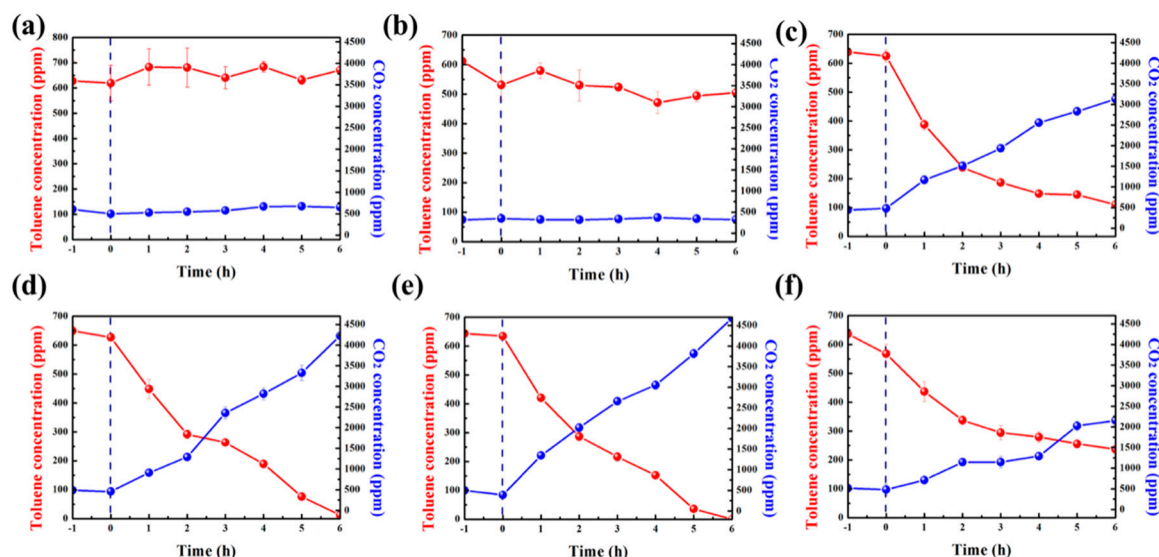

Figure 6. The degradation results to 665 ppm toluene of (**a**) blank (**b**) TCN IO adsorption (in dark) (**c**) bulk-TiO$_2$, (**d**) TiO$_2$ IO, (**e**)TCN IO (**f**) P25 under simulated sunlight irradiation.

Under the irradiation of simulated solar light, samples were also used for the degradation of liquid phase pollutants represented by RhB and phenol. As shown in Figure 7, the degradation rate of dye and phenol reached above 97% after 75 min and 100 min of illumination, respectively. The efficient degradation of phenol and RhB provides evidence of the high performance of TCN IO and proves that as-prepared catalysts could also be utilized to solve the problem of water pollution.
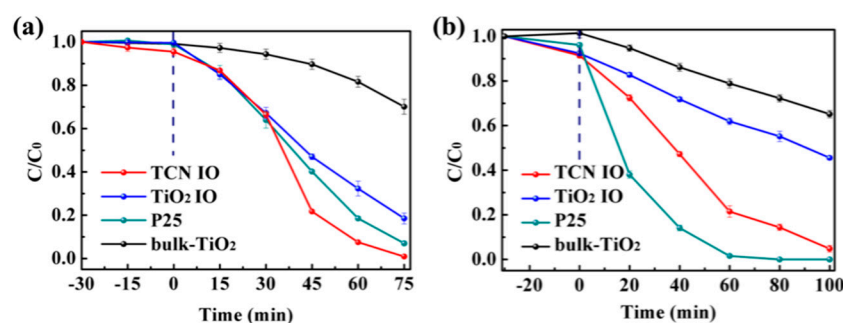
Figure 7. Photocatalytic degradation results to (**a**) 20 mg/L of RhB and (**b**) 10 mg/L phenol over TCN IO under simulated sunlight irradiation.

The reusability and stability of the catalyst is an important parameter to evaluate its practical application potential. After illuminating the substrates by a solar simulator (AM 1.5) equipped with a 300 W Xenon lamp for 30 min and overnight ventilating without washing, the catalyst was recycled. The recycling experiment was repeated four times to test the stability of TCN IO for toluene degradation. As shown in Figure 8, a near 88% degradation ratio of 665 ppm toluene can be observed in the fourth degradation process, revealing the excellent reusability and stability of the as-prepared catalyst TCN IO. Figure S2 shows XRD of TCN IO sample after the recycle experiments had been conducted (Figure S2). The slight decrease in crystallinity and part of the toluene which occupies the active sites of the catalyst and partially inhibits the reaction, probably caused the monotonous but small drop in activity.
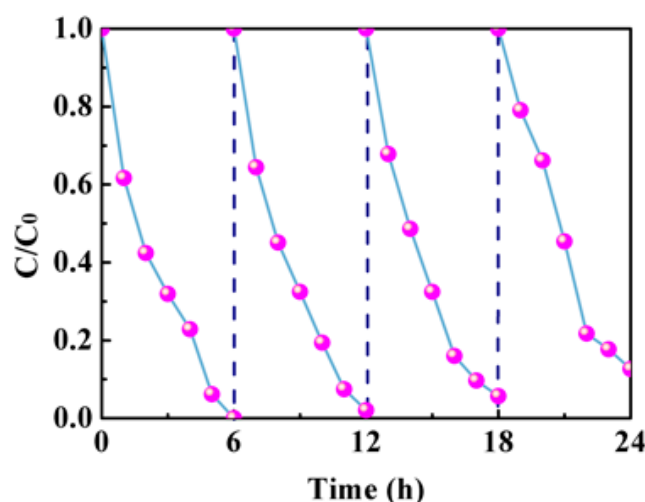

Figure 8. Recycle experiment tests of TCN IO for degrading 665 ppm toluene under simulated solar light irradiation.

3. Materials and Methods

3.1. Synthesis of PS Colloidal Crystal Template

Polystyrene spheres (PS) suspension with controllable size were synthesized according to the reported emulsion polymerization method [20,23–25]. Styrene monomers were alternately washed with 0.5 M NaOH solution and deionized water in a separate funnel with a 1:1 volume ratio 3 times to remove the polymerization inhibitor in styrene. 0.45 g of sodium dodecyl sulfate (SDS) and 0.6 g of $K_2S_2O_8$ were mixed in 288 mL of deionized water and 32 mL of ethanol (EtOH) with magnetic stirring to form a homogeneous solution; this was followed by injecting 36 mL of washed styrene at nitrogen atmosphere. A milky product was obtained after heating at 71 °C for 19 h. The as-prepared polystyrene emulsion

was transferred into 250 mL beakers with a height of ~ 2 cm and then put into a 70 °C oven to evaporate the solvent.

3.2. Synthesis of Graphitic Carbon Nitride Quantum Dots (CNQDs)

CNQDs were synthesized through a simple low-temperature solid-phase method as reported [42]. 0.101 g of urea and 0.081 g of sodium citrate were mixed and grounded to powders in an agate mortar, then the mixture was transferred into a Teflon-lined stainless-steel autoclave (20 mL capacity) and followed by thermal treatment at 180 °C for 2 h in an oven. The resultant mixture was alternately washed with ethanol and centrifuged three times (12,000 rpm for 10 min). A yellowish CNQDs solution was obtained by dialyzing against 20 mL of deionized water through a dialysis membrane with 3500 molecule weight cut-off (MWCO) for 24 h.

3.3. Synthesis of TiO_2 IO and TCN IO

The synthesis process of CNQDs incorporated TiO_2 inverse opal (TCN IO) is shown in Figure 9. In detail, 5.6 mL of titanium isopropoxide (TTIP), 45 mL of EtOH and 1 mL of acetylacetone (AcAc) were mixed and stirred. Then, 0.85 mL of hydrochloric acid and 4.6 mL of CNQDs aqueous solution were added into the solution, which was continually stirred for 2 h. Then the precursor solution was dropped on the PS colloidal crystal solids. After hydrolysis for 8 h at room temperature, the samples were calcined at 500 °C for 2 h (heating rate was 2 °C/min). On the other hand, pure TiO_2 inverse opals (TiO_2 IO) were prepared via the same method by replacing CNQDs with 5 mL of deionized water in precursor solution. Additionally, bulk-TiO_2 was synthesized without templates by using the same precursor solution as TiO_2 IO.
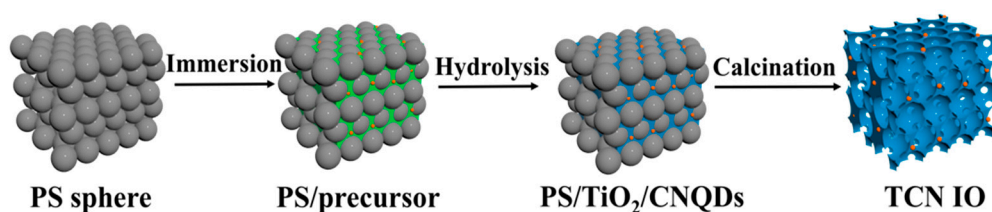

Figure 9. Synthesis process of TCN IO.

3.4. Characterization of Materials

X-ray diffraction (XRD) was conducted with a Shimadzu XRD-7000 XRD diffractometer (Shimadzu, Kyoto, Japan) using Cu Kα (λ= 0.15406 nm) radiation. Other test conditions included a current of 100 mA, an operating voltage of 40 kV, a scanning range between 2θ = 5–75° and a scan rate of 0.02°/2 s. Scanning electron microscopy (SEM) was conducted by a JSM-6360 LV electron microscope (Jeol, Tokyo, Japan). A routine analysis consisted of sprinkling the sample on a conductive tape and spraying with gold under a 15 kV work voltage. The transmission electron microscopy (TEM), which was used to characterize the samples' morphologies, was performed on a Jeol JEM-2011 transmission electron microscope (Jeol, Tokyo, Japan) with a 120–200 kV work voltage. The morphologies of commercial and homemade TiO_2-based samples were further characterized by HRTEM using a Jeol JEM-2100 (Jeol, Tokyo, Japan). X-ray photoelectron spectroscopy (XPS) was tested with a PerkinElmer PHI 5000C ESCA system(PerkinElmer, Waltham, MA, USA) with Al K radiation (250 W). The Brunauer−Emmett−Teller (BET) surface area of all photocatalysts was obtained via nitrogen adsorption at 77 K by a Micromeritics ASAP2010 (Micromeritics, Norcross, GA, USA). The photoluminescence (PL) spectra of samples were measured with a RF-5301 spectrofluorophotometer (Shimadzu, Kyoto, Japan). With an electrochemical analyzer CHI 660 D electrochemical station (CH Instruments Inc., Bee Cave, TX, USA), the electrochemical experiments were carried out in a cell with a standard three-electrode system. It consisted of a working electrode (as-prepared samples

were coated on a square fluoride-tin oxide (FTO) with an area of ca. $0.5\ cm^{-2}$), a Pt wire serving as the counter electrode and a saturated Ag/AgCl acting as the reference electrode. Electrochemical impedance spectroscopy (EIS) of different samples were obtained in the frequency range from 100 kHz to 0.1 Hz under an amplitude of 10 mV using N_2-saturated potassium ferricyanide-mixed electrolyte.

3.5. Photocatalytic Degradation of VOCs and Dyes

The photocatalytic activities of the prepared photocatalysts were evaluated by the degradations of the gas phase VOCs toluene, the liquid phase VOCs phenol and a typical dye RhB under simulated sunlight irradiation. The photocatalytic reactions were conducted under simulated solar light by a 300 W Xe lamp CEL-HXF300 (Beijing Jin Yuan Technology Co., Beijing, China) with a cut-off filter (AM 1.5), of which the UV-Visible emission spectrum is 350–780 nm.

In the case of photocatalytic degradation of toluene, the distance between the light source and the substrate coated with photocatalysts was 20 cm where the light intensity was $612\ mW/cm^2$. For preparation of the substrate, 100 mg of photocatalyst was dispersed in 3.5 mL of EtOH via sonication for 15 min and the obtained suspension was slowly and evenly dropped on a square quartz substrate with an area of $64\ cm^2$. The substrate was deposited in a 70 °C oven over night for drying and stabilization. A self-developed Pyrex reactor (total volume of 1.735 L) with a flat quartz window on the top was used, wherein the prepared substrate was placed on a quartz holder inside the reactor (Figure S3). The reactor was sealed and flushed with air for 30 min, and then 5 μL of liquid toluene were injected into the reactor in a vacuum state and vaporized into gas phase, which corresponded to the initial concentration of 665 ppm ($2500\ mg/m^3$). Before the lamp was switched on, the gas–solid adsorption equilibrium was reached after 1 h. The photocatalytic oxidation of toluene was evaluated by toluene and CO_2 detection at different time intervals on a Inesa GC126N gas chromatograph (Inesa Analytical Istrument Co., Shanghai, China) equipped with a flame ionization detector (FID), and a methane-reforming furnace [44]. The adsorption efficiency of toluene ($\xi_{t,\ toluene}$) in the dark condition and the photocatalytic degradation efficiencies of toluene into CO_2 ($\blacksquare_{t,\ toluene}$) over different photocatalysts were calculated according to the following formulas:

$$\xi_{t,\ toluene} = 1 - C_{t,\ C7H8}\ /C_{0,\ C7H8}, \tag{1}$$

$$\blacksquare_{t,\ toluene} = (C_{t,\ CO2} - C_{0,\ CO2})/7C_{0,\ C7H8}, \tag{2}$$

where $C_{0,\ C7H8}$ and $C_{0,\ CO2}$ are the initial concentrations of C_7H_8 and CO_2, respectively, $C_{t,\ C7H8}$ and $C_{t,\ C7H8}$ are the concentrations of C_7H_8 and CO_2 at reaction time (t), respectively.

For the degradation of phenol and RhB, 50 mg of photocatalyst was added into a quartz reactor containing 50 mL of 10 mg/L phenol solution and 20 mg/L RhB, respectively. Prior to the photocatalytic reaction, the suspension was stirred for 30 min in the dark to achieve the adsorption-desorption equilibrium of organic contaminants on the surface of the catalysts. At the given time interval, the analytical sample was taken from the mixture solution and immediately centrifuged. The concentrations of phenol were analyzed by a Shimadzu SPD-M20A (Shimadzu, Kyoto, Japan) high-performance liquid chromatograph (HPLC), while those of RhB were measured with a Shimadzu 2450 UV-vis spectrophotometer (Shimadzu, Kyoto, Japan).

All tests of photocatalytic activities over samples were conducted three times and the mean values were reported. No significant deviations between the three tests were found.

4. Conclusions

In this study, carbon nitride quantum dots for in situ-loading TiO_2 inverse opal structures were designed and prepared for photocatalytic degradation of gaseous toluene under simulated sunlight irradiation. Compared with the common catalyst bulk-TiO_2, TiO_2 IO and commercial P25, the as-prepared TCN IO significantly promoted the degradation

of toluene, and a 93% mineralization rate of 665 ppm toluene was achieved within 6 h. The small material can be used for the degradation of liquid phase pollutants such as RhB and phenol. Based on the specific surface area, photoelectrochemical measurements and PL spectra, it can be concluded that the modification of CNQDs and inverse opals structure not only increases the surface area, along with the concentration of active sites, but also decreases the recombination rate of photo-generated electrons and holes. This material, with good stability and green environmental protection, provides a practical solution to the problem of indoor toxic VOCs pollution and wastewater treatment.

Supplementary Materials: The following are available online at https://www.mdpi.com/article/10.3390/catal11040464/s1, Figure S1: SEM image of (a) PS template (b) TiO_2 IO, Figure S2: X-ray diffraction (XRD) of TCN IO, Figure S3: Reactor device, Table S1: The comparison of the photocatalytic degradation efficiencies of toluene into CO_2 (■t, toluene) over different samples.

Conflicts of Interest: The authors declare no conflict of interest. The funders had no role in the design of the study; in the collection, analyses, or interpretation of data; in the writing of the manuscript, or in the decision to publish the results.

References

1. Nazaroff, W.W. Exploring the consequences of climate change for indoor air quality. *Environ. Res. Lett.* **2013**, *8*, 15022. [CrossRef]
2. Mamaghani, A.H.; Haghighat, F.; Lee, C.-S. Photocatalytic oxidation technology for indoor environment air purification: The state-of-the-art. *Appl. Catal. B Environ.* **2017**, *203*, 247–269. [CrossRef]
3. Paul, T.; Sree, D.; Aglan, H. Effect of mechanically induced ventilation on the indoor air quality of building envelopes. *Energy Build.* **2010**, *42*, 326–332. [CrossRef]
4. Boyjoo, Y.; Sun, H.; Liu, J.; Pareek, V.K.; Wang, S. A review on photocatalysis for air treatment: From catalyst development to reactor design. *Chem. Eng. J.* **2017**, *310*, 537–559. [CrossRef]
5. Thompson, T.; Webber, M.; Allen, D.T. Air quality impacts of using overnight electricity generation to charge plug-in hybrid electric vehicles for daytime use. *Environ. Res. Lett.* **2009**, *4*, 14002. [CrossRef]
6. Takeuchi, M.; Hidaka, M.; Anpo, M. Efficient removal of toluene and benzene in gas phase by the TiO_2/Y-zeolite hybrid photocatalyst. *J. Hazard. Mater.* **2012**, *237*, 133–139. [CrossRef] [PubMed]
7. Zhang, X.; Gao, B.; Creamer, A.E.; Cao, C.; Li, Y. Adsorption of VOCs onto engineered carbon materials: A review. *J. Hazard. Mater.* **2017**, *338*, 102–123. [CrossRef] [PubMed]
8. Chen, G.; Wang, Z.; Lin, F.; Zhang, Z.; Yu, H.; Yan, B.; Wang, Z. Comparative investigation on catalytic ozonation of VOCs in different types over supported MnOx catalysts. *J. Hazard. Mater.* **2020**, *391*, 122218. [CrossRef] [PubMed]
9. Chunyu, C.; Tong, L.; Hui, W.; Qinqin, Y.U.; Jie, F.A.N.; Liping, X.; ZHENG, X. Removal of hexanal by non-thermal plasma and MnOx/γ-Al$_2$O$_3$ combination. *Chin. J. Catal.* **2012**, *33*, 941–951.
10. Tyagi, A.; Matsumoto, T.; Yamamoto, A.; Kato, T.; Yoshida, H. Metal Cocatalyst Directing Photocatalytic Acetonylation of Toluene via Dehydrogenative Cross-Coupling with Acetone. *Catal. Lett.* **2020**, *150*, 31–38. [CrossRef]
11. Mo, J.; Zhang, Y.; Xu, Q. Effect of water vapor on the by-products and decomposition rate of ppb-level toluene by photocatalytic oxidation. *Appl. Catal. B Environ.* **2013**, *132*, 212–218. [CrossRef]
12. Eftekhari, E.; Broisson, P.; Aravindakshan, N.; Wu, Z.; Cole, I.S.; Li, X.; Zhao, D.; Li, Q. Sandwich-structured TiO_2 inverse opal circulates slow photons for tremendous improvement in solar energy conversion efficiency. *J. Mater. Chem. A* **2017**, *5*, 12803–12810. [CrossRef]
13. Liu, L.; Karuturi, S.K.; Su, L.T.; Tok, A.I.Y. TiO_2 inverse-opal electrode fabricated by atomic layer deposition for dye-sensitized solar cell applications. *Energy Environ. Sci.* **2011**, *4*, 209–215. [CrossRef]
14. Zhao, H.; Hu, Z.; Liu, J.; Li, Y.; Wu, M.; Van Tendeloo, G.; Su, B.-L. Blue-edge slow photons promoting visible-light hydrogen production on gradient ternary 3DOM TiO_2-Au-CdS photonic crystals. *Nano Energy* **2018**, *47*, 266–274. [CrossRef]
15. Schroden, R.C.; Al-Daous, M.; Blanford, C.F.; Stein, A. Optical properties of inverse opal photonic crystals. *Chem. Mater.* **2002**, *14*, 3305–3315. [CrossRef]

16. Wu, M.; Liu, J.; Jin, J.; Wang, C.; Huang, S.; Deng, Z.; Li, Y.; Su, B.-L. Probing significant light absorption enhancement of titania inverse opal films for highly exalted photocatalytic degradation of dye pollutants. *Appl. Catal. B Environ.* **2014**, *150*, 411–420. [CrossRef]

17. Zalfani, M.; Van Der Schueren, B.; Hu, Z.-Y.; Rooke, J.C.; Bourguiga, R.; Wu, M.; Li, Y.; Van Tendeloo, G.; Su, B.-L. Novel 3DOM BiVO$_4$/TiO$_2$ nanocomposites for highly enhanced photocatalytic activity. *J. Mater. Chem. A* **2015**, *3*, 21244–21256. [CrossRef]

18. Phillips, K.R.; England, G.T.; Sunny, S.; Shirman, E.; Shirman, T.; Vogel, N.; Aizenberg, J. A colloidoscope of colloid-based porous materials and their uses. *Chem. Soc. Rev.* **2016**, *45*, 281–322. [CrossRef]

19. Zheng, X.; Yang, Y.; Chen, S.; Zhang, L. Slow photons for solar fuels. *Chin. J. Catal.* **2018**, *39*, 379–389. [CrossRef]

20. Qi, D.; Lu, L.; Wang, L.; Zhang, J. Improved SERS sensitivity on plasmon-free TiO$_2$ photonic microarray by enhancing light-matter coupling. *J. Am. Chem. Soc.* **2014**, *136*, 9886–9889. [CrossRef]

21. Liang, Z.; Zheng, G.; Li, W.; Seh, Z.W.; Yao, H.; Yan, K.; Kong, D.; Cui, Y. Sulfur cathodes with hydrogen reduced titanium dioxide inverse opal structure. *ACS Nano* **2014**, *8*, 5249–5256. [CrossRef] [PubMed]

22. Cho, C.-Y.; Lee, S.; Lee, J.; Lee, D.C.; Moon, J.H. Tetrapod CdSe-sensitized macroporous inverse opal electrodes for photo-electrochemical applications. *J. Mater. Chem. A* **2014**, *2*, 17568–17573. [CrossRef]

23. Lu, L.; Teng, F.; SenTapas; Qi, D.; Wang, L.; Zhang, J. Synthesis of visible-light driven CrxOy-TiO$_2$ binary photocatalyst based on hierarchical macro-mesoporous silica. *Appl. Catal. B Environ.* **2015**, *163*, 9–15. [CrossRef]

24. Zhou, L.; Lei, J.; Wang, L.; Liu, Y.; Zhang, J. Highly efficient photo-Fenton degradation of methyl orange facilitated by slow light effect and hierarchical porous structure of Fe$_2$O$_3$-SiO$_2$ photonic crystals. *Appl. Catal. B Environ.* **2018**, *237*, 1160–1167. [CrossRef]

25. Qi, D.; Lu, L.; Xi, Z.; Wang, L.; Zhang, J. Enhanced photocatalytic performance of TiO$_2$ based on synergistic effect of Ti$_3$+ self-doping and slow light effect. *Appl. Catal. B Environ.* **2014**, *160*, 621–628. [CrossRef]

26. Bertolini, G.R.; Pizzio, L.R.; Kubacka, A.; Muñoz-Batista, M.J.; Fernández-García, M. Composite H$_3$PW$_{12}$O$_{40}$–TiO$_2$ catalysts for toluene selective photo-oxidation. *Appl. Catal. B Environ.* **2018**, *225*, 100–109. [CrossRef]

27. Obee, T.N.; Brown, R.T. TiO$_2$ photocatalysis for indoor air applications: Effects of humidity and trace contaminant levels on the oxidation rates of formaldehyde, toluene, and 1,3-butadiene. *Environ. Sci. Technol.* **1995**, *29*, 1223–1231. [CrossRef]

28. Sun, J.; Li, X.; Zhao, Q.; Ke, J.; Zhang, D. Novel V$_2$O$_5$/BiVO$_4$/TiO$_2$ nanocomposites with high visible-light-induced photocatalytic activity for the degradation of toluene. *J. Phys. Chem. C* **2014**, *118*, 10113–10121. [CrossRef]

29. Li, H.; Shen, X.; Liu, Y.; Wang, L.; Lei, J.; Zhang, J. Facile phase control for hydrothermal synthesis of anatase-rutile TiO2 with enhanced photocatalytic activity. *J. Alloys Compd.* **2015**, *646*, 380–386. [CrossRef]

30. Xu, P.; Shen, X.; Luo, L.; Shi, Z.; Liu, Z.; Chen, Z.; Zhu, M.; Zhang, L. Preparation of TiO$_2$/Bi$_2$WO$_6$ nanostructured heterojunctions on carbon fibers as a weaveable visible-light photocatalyst/photoelectrode. *Environ. Sci. Nano* **2018**, *5*, 327–337. [CrossRef]

31. Zhou, L.; Wang, L.; Lei, J.; Liu, Y.; Zhang, J. Fabrication of TiO$_2$/Co-g-C$_3$N$_4$ heterojunction catalyst and its photocatalytic performance. *Catal. Commun.* **2017**, *89*, 125–128. [CrossRef]

32. Zhao, Z.; Sun, Y.; Dong, F. Graphitic carbon nitride based nanocomposites: A review. *Nanoscale* **2015**, *7*, 15–37. [CrossRef] [PubMed]

33. Wang, X.; Maeda, K.; Thomas, A.; Takanabe, K.; Xin, G.; Carlsson, J.M.; Domen, K.; Antonietti, M. A metal-free polymeric photocatalyst for hydrogen production from water under visible light. *Nat. Mater.* **2009**, *8*, 76–80. [CrossRef] [PubMed]

34. Liu, F.; Yu, J.; Tu, G.; Qu, L.; Xiao, J.; Liu, Y.; Wang, L.; Lei, J.; Zhang, J. Carbon nitride coupled Ti-SBA15 catalyst for visible-light-driven photocatalytic reduction of Cr (VI) and the synergistic oxidation of phenol. *Appl. Catal. B Environ.* **2017**, *201*, 1–11. [CrossRef]

35. Lei, J.; Chen, Y.; Shen, F.; Wang, L.; Liu, Y.; Zhang, J. Surface modification of TiO$_2$ with g-C$_3$N$_4$ for enhanced UV and visible photocatalytic activity. *J. Alloys Compd.* **2015**, *631*, 328–334. [CrossRef]

36. Li, H.; Zhou, L.; Wang, L.; Liu, Y.; Lei, J.; Zhang, J. In situ growth of TiO$_2$ nanocrystals on g-C$_3$N$_4$ for enhanced photocatalytic performance. *Phys. Chem. Chem. Phys.* **2015**, *17*, 17406–17412. [CrossRef]

37. Curry, D.E.; Andrea, K.A.; Carrier, A.J.; Nganou, C.; Scheller, H.; Yang, D.; Youden, B.; Zhang, Y.; Nicholson, A.; Cui, S.; et al. Surface interaction of doxorubicin with anatase determines its photodegradation mechanism: Insights into removal of waterborne pharmaceuticals by TiO$_2$ nanoparticles. *Environ. Sci. Nano* **2018**, *5*, 1027–1035. [CrossRef]

38. Lei, J.; Liu, F.; Wang, L.; Liu, Y.; Zhang, J. A binary polymer composite of graphitic carbon nitride and poly (diphenylbutadiyne) with enhanced visible light photocatalytic activity. *RSC Adv.* **2017**, *7*, 27377–27383. [CrossRef]

39. Jin, X.; Balasubramanian, V.V.; Selvan, S.T.; Sawant, D.P.; Chari, M.A.; Lu, G.E.; Vinu, A. Highly ordered mesoporous carbon nitride nanoparticles with high nitrogen content: A metal-free basic catalyst. *Angew. Chemie Int. Ed.* **2009**, *48*, 7884–7887. [CrossRef]

40. Peng, Y.; Wang, L.; Liu, Y.; Chen, H.; Lei, J.; Zhang, J. Visible-Light-Driven Photocatalytic H$_2$O$_2$ Production on g-C$_3$N$_4$ Loaded with CoP as a Noble Metal Free Cocatalyst. *Eur. J. Inorg. Chem.* **2017**, *2017*, 4797–4802. [CrossRef]

41. Zhou, L.; Tian, Y.; Lei, J.; Wang, L.; Liu, Y.; Zhang, J. Self-modification of gC 3 N 4 with its quantum dots for enhanced photocatalytic activity. *Catal. Sci. Technol.* **2018**, *8*, 2617–2623. [CrossRef]

42. Zhou, J.; Yang, Y.; Zhang, C. A low-temperature solid-phase method to synthesize highly fluorescent carbon nitride dots with tunable emission. *Chem. Commun.* **2013**, *49*, 8605–8607. [CrossRef]

43. Yu, J.; Lei, J.; Wang, L.; Zhang, J.; Liu, Y. TiO$_2$ inverse opal photonic crystals: Synthesis, modification, and applications—A review. *J. Alloys Compd.* **2018**, *769*, 740–757. [CrossRef]

44. Qian, X.; Ren, M.; Yue, D.; Zhu, Y.; Han, Y.; Bian, Z.; Zhao, Y. Mesoporous TiO_2 films coated on carbon foam based on waste polyurethane for enhanced photocatalytic oxidation of VOCs. *Appl. Catal. B Environ.* **2017**, *212*, 1–6. [CrossRef]

45. Sun, L.; Yang, M.; Huang, J.; Yu, D.; Hong, W.; Chen, X. Freestanding Graphitic Carbon Nitride Photonic Crystals for Enhanced Photocatalysis. *Adv. Funct. Mater.* **2016**, *26*, 4943–4950. [CrossRef]

46. Su, J.; Zhu, L.; Geng, P.; Chen, G. Self-assembly graphitic carbon nitride quantum dots anchored on TiO_2 nanotube arrays: An efficient heterojunction for pollutants degradation under solar light. *J. Hazard. Mater.* **2016**, *316*, 159–168. [CrossRef] [PubMed]

47. Fang, Q.; Meier, M.; Yu, J.J.; Wang, Z.M.; Zhang, J.Y.; Wu, J.X.; Kenyon, A.; Hoffmann, P.; Boyd, I.W. FTIR and XPS investigation of Er-doped SiO_2-TiO_2 films. *Mater. Sci. Eng. B Solid-State Mater. Adv. Technol.* **2003**, *105*, 209–213. [CrossRef]

48. Su, J.; Zhu, L.; Chen, G. Ultrasmall graphitic carbon nitride quantum dots decorated self-organized TiO_2 nanotube arrays with highly efficient photoelectrochemical activity. *Appl. Catal. B Environ.* **2016**, *186*, 127–135. [CrossRef]

49. Zhuang, Z.; Li, Y.; Li, Z.; Lv, F.; Lang, Z.; Zhao, K.; Zhou, L.; Moskaleva, L.; Guo, S.; Mai, L. MoB/g-C_3N_4 Interface Materials as a Schottky Catalyst to Boost Hydrogen Evolution. *Angew. Chem. Int. Ed.* **2018**, *57*, 496–500. [CrossRef]